Available online at www.sciencedirect.com
SCIENCE DIRECT®
Pergamon
Acta Materialia 51 (2003) 4719–4735
Acta MATERIALIA
www.actamat-journals.com

On the influence of the grain boundary misorientation on the plastic deformation of aluminum bicrystals

S. Zaefferer [a], J.-C. Kuo [a], Z. Zhao [a,1], M. Winning [b], D. Raabe [a,*]

[a] *Microstructure Physics, Max-Planck-Institut für Eisenforschung, Max-Planck-Str. 1, 40237 Düsseldorf, Germany*
[b] *Institut für Metallkunde und Metallphysik, Kopernikusstr. 14, RWTH Aachen, 52056 Aachen, Germany*

Received 6 September 2002; received in revised form 8 May 2003; accepted 9 May 2003

Abstract

Aluminum bicrystals with symmetric ⟨1 1 2⟩ tilt boundaries and misorientations of 8.7° (small angle), 15.4° (transition), and 31.5° (large angle) were deformed in a channel die experiment in order to study the influence of misorientation on the deformation at grain boundaries. Samples were characterized by strain measurements and microtexture mappings. The experiments were compared to crystal plasticity finite element simulations. We studied strain heterogeneity at the macroscopic and at the microscopic level. Even macroscopically homogeneous areas showed microscopic heterogeneity in the form of bands of different sets of glide systems. We observed clear effects of the grain boundary misorientation on the deformation kinematics close to the boundaries. The 8.7° grain boundary did not show any orientation change which was interpreted in terms of free dislocation penetration. In contrast, the 15.4° and 31.5° bicrystals showed orientation changes which were attributed to dislocation pile-ups.

Keywords: Crystallographic texture; Deformation; Bicrystal; Modeling; Aluminum

1. Introduction

1.1. Problem formulation

The current work is an experimental and theoretical study on deformed aluminum bicrystals. We aim at better understanding the role of grain boundaries of different misorientations during plastic deformation. Grain boundaries act as obstacles to dislocation motion during deformation entailing an increase in yield strength with decreasing grain size as expressed by the Hall–Petch relation. The mechanical effect of a grain boundary depends on its misorientation. Small angle grain boundaries (with misorientations of up to 15–20°) are weak obstacles to the plastic flow when compared to large angle grain boundaries because they can be penetrated by dislocations which continue their glide path in the neighboring crystal. However, since small angle grain boundaries themselves consist of dislocations, the interaction with mobile dislocations may gradually change their

* Corresponding author. Tel.: +49-211-679-2278; fax: +49-211-679-2333.
E-mail address: raabe@mpie.de (D. Raabe).
[1] Now at: Massachusetts Institute of Technology, 77 Massachusetts Avenue, Cambridge, MA 02139-4307, USA.

1359-6454/$30.00 © 2003 Acta Materialia Inc. Published by Elsevier Ltd. All rights reserved.
doi:10.1016/S1359-6454(03)00259-3

structure and misorientation during plastic straining.

In order to study these effects in quantitative detail and derive from them an improved understanding of inter- and intragranular strain heterogeneity inherent to polycrystal plasticity [1–4], we investigate in this work a set of bicrystals with different well defined grain boundaries during deformation.

1.2. Related previous work on bicrystal plasticity

In the literature, the deformation of bicrystals of different materials has been studied extensively. Detailed investigations have been carried out, for instance, on tin [5], zinc [6,7], aluminum [8–15], silver [16], magnesium [17], Fe–3%Si [18,19], β-brass [20,21] and copper [22].

Livingston and Chalmers [10], like many other early authors in this field, concluded from their work on aluminum bicrystals that, in order to keep the macroscopic plastic compatibility across the grain boundary, bicrystals have to deform by multiple slip. Hook and Hirth [18,19] suggested in their studies on Fe–3%Si bicrystals that the elastic incompatibility at the grain boundaries results in the activation of secondary slip systems. While these early investigations had built their discussions essentially on *intergranular* incompatibility assuming otherwise homogeneous behavior of the two abutting crystals, more recent detailed studies by Rey and Zaoui [13,22] revealed that the presence of grain boundaries can also give rise to considerable *intragranular* heterogeneity. Rey and Zaoui found that intragranular nonhomogeneity leads to internal stresses inside each of the two neighboring crystals entailing activation of additional slip systems and considerable corresponding hardening effects. Sun et al. [14] inspected strain heterogeneity in the vicinity of grain boundaries in even greater detail using orientation imaging microscopy via scanning electron microscopy. In their analysis, they applied the concept of Kröner's geometrically necessary dislocation tensor [23] to the description of lattice curvature near the grain boundary in a plastically strained aluminum bicrystal.

1.3. Related previous work on aluminum single crystal plasticity

Much related work was also devoted to the study of the plastic deformation of aluminum single crystals. As we will see in the following, these results are of considerable relevance for the interpretation of bicrystal mechanics. We refer in particular to the recent work of the groups of Hansen [24–27] and Driver [28,29].

Wert et al. [24] investigated the microtexture of a cube-oriented aluminum single crystal deformed 30% by rolling using EBSP and TEM. They observed that the deformed crystal was subdivided into macroscopic bands parallel to the rolling plane as well as dislocation cells and cell blocks at the microscopic scale. Crystallite rotations occurred predominantly about the transverse direction. A Schmid factor analysis of plane strain compression revealed that four slip systems were active during deformation, forming two co-directional pairs of slip dyads. Godfrey et al. [25] investigated the evolution of microstructure and texture in pure aluminum single crystals of $(1\,1\,0)\langle 1\bar{1}\,2\rangle$ orientation deformed by channel die. The authors observed a homogeneous cell block deformation microstructure at low strains. At higher strain, the cell blocks were less distinct and strain localization occurred. Hansen and Huang [26] investigated the relationship between polycrystal and single crystal deformation for aluminum at different strains using TEM. The authors investigated 89 different grains. They established three basic types of deformation microstructures which they correlated to the grain orientation. The behavior of the grains embedded in the polycrystal were compared with the behavior of single crystals. Godfrey et al. [27] studied the effect of deformation microstructure heterogeneity on recrystallization using channel die deformed single crystals of typical rolling texture components. In their work, the authors found a wide range of spatial and orientational heterogeneity, which they related to the crystal orientation. Maurice and Driver [28] investigated the influence of the deformation temperature on the hot rolling textures of aluminum polycrystals and single crystals. In their work, the authors found that their texture and microstructure observations could be interpreted in

terms of the onset of non-octahedral slip. Basson and Driver [29] studied channel die deformed cube-oriented aluminum single crystals up to strains of 1.5. Slip trace analysis and texture measurement by EBSD showed that coarse deformation banding was initiated in the form of rotations about the transverse direction. Other rotations were also found about the rolling direction.

1.4. Basic motivation and plan of the investigation

Despite the excellence of the quoted studies it is difficult to draw systematic conclusions from them on the influence of the grain boundary misorientation on bicrystal micromechanics and microtexture. This is essentially due to the different materials (stacking-fault energy, anisotropy of elasticity), samples (initial orientations, misorientations across the grain boundaries), and deformation modes (loading, friction) tackled in these investigations. Therefore, in the present work a systematic study was carried out on three aluminum bicrystals with different symmetric tilt boundaries with misorientations of 8.7°, 15.4°, and 31.5° that have been deformed in a channel die experiment.

The best way to observe dislocation interactions is certainly offered by TEM where lattice and boundary dislocations and their reaction products can be observed directly. However, TEM also exhibits some important drawbacks for such observations. TEM sample preparation is destructive, i.e. deformation experiments can usually not be continued after a TEM observation. Additionally, the areas observed in the TEM are usually rather small and may not be representative for the whole specimen. Finally, the preparation of thin foils for TEM may lead to a change in dislocation structure and may, therefore, not reflect the bulk microstructure.

For these reasons, we employ in our study the technique of automated crystal orientation mapping (ACOM) using automatic evaluation of electron backscatter diffraction (EBSD) patterns in the SEM. This technique offers the possibility to study the evolution of microstructure and lattice rotation in the course of a deformation experiment on bulk samples without any interference with the deformation process. Although the ACOM technique does not directly reveal the dislocation structure of the material, the precise measurement of local lattice orientation with high spatial resolution may be interpreted in terms of dislocation arrangements. This task has become particularly feasible with the advance of ACOM in a high resolution SEM with thermal field emitter (FEGSEM).

Similar to TEM, high resolution ACOM measurements only allow the observation of relatively small areas. This is a great problem in the case of a heterogeneous strain distribution and it will become clear in the course of this work that the channel die deformation mode that has been adapted here is an experiment which creates strain heterogeneity. Therefore, we used other experimental techniques to characterize the macroscopic deformation heterogeneity of the deformation experiments. First, a photogrametric method was applied to determine the macroscopic distribution of the accumulated plastic surface strains. Second, large, low resolution orientation maps were measured by ACOM. Finally, a crystal elasticity–plasticity finite element model (CPFEM) was used to better understand the origin of the evolution of strain heterogeneities and gain an insight into the activated glide systems and crystal rotations. The CPFEM results were compared to predictions obtained by crystal plasticity homogenization techniques. Besides the details mentioned above, another important goal of the plasticity modeling consisted of separating the mechanisms occurring in deformation zones close to a grain boundary from those occurring in the bulk far away from a grain boundary.

It is clear that a changing grain boundary misorientation is always linked to a change in the orientations of one or both of the two abutting crystals. This means that the observed changes in microstructure and texture evolution for different bicrystals are only to a small part due to the changing grain boundary structure, but mainly due to the change of crystal orientation. The used finite element deformation model, of course, does not include any constitutive description of the grain boundary structure and its mechanical effect. This means that the model does not have any *knowledge*

of the grain boundary structure and, therefore, can only predict effects which stem from crystal kinematics and from the elasto-viscoplastic dynamics of the bulk material. We, therefore, conduct a critical comparison of the simulation results with the experimental observations in order to identify the actual effects which originate from the grain boundary in the experimental data.

There are, in conclusion, several questions to be addressed in this work. The first interest is to improve our understanding of the role of grain boundaries and their misorientation in polycrystal deformation. The next question is, how in a bicrystal deformation experiment grain boundary and bulk deformation effects can be separated and in how far simulations can be of help in this context. A last question addresses the experimental and theoretical characterization of strain heterogeneity in the case of channel die deformation of bicrystals.

2. Experimental

2.1. Sample preparation and channel die compression experiments

Aluminum bicrystals were grown from 99.999% pure material using a modified Bridgman technique with seed crystals of pre-selected orientations [30,31]. Three bicrystals with symmetrical $\langle 1\,1\,2\rangle$ tilt boundaries with 8.7°, 15.4°, and 31.5° misorientation across the grain boundary were used for the experiments. The sample size for the channel die compression experiments was in all cases about $17 \times 19 \times 4$ mm^3. The geometry and dimensions with respect to the channel die experiment are shown in Fig. 1a. In correspondence to conventional rolling deformation, the reference coordinates are referred to as rolling direction (RD) for the free elongation direction, transverse direction (TD) for the direction constrained by the channel die, and normal direction (ND) for the compression direction. The grain boundary normal (GBN) was chosen to be parallel to the compression axis as shown in Fig. 1a. The initial orientations of the bicrystals were measured using electron backscatter diffraction. They are displayed in (1 1 1) pole figures in Fig. 1b.

After the samples had been polished from all sides, a stochastic color spray pattern for photogrametric measurements (see next section) was placed on the TD surface. Plane strain compression experiments were then conducted at a strain rate of 1.7×10^{-5} s^{-1} using a channel die set-up as shown in Fig. 1a. Plastic deformation was applied in a sequence of loading steps, each imposing a plastic strain of about 5% reduction up to a total plastic thickness reduction of 30%. In order to reduce frictional effects and to protect the color spray pattern on the specimen surface, the specimens were wrapped with several layers of an 80 μm thick teflon foil.

2.2. Experimental determination of accumulated plastic microstrains by photogrametry

The determination of the plastic displacement field and the subsequent calculation of some tensor components of the plastic strain field was, after each deformation step, conducted by applying a photogrametric procedure to the TD surface of the strained bicrystals. Photogrametry is a digital image analysis method which is based on the recognition of geometrical changes in the gray scale distribution of surface patterns before and after straining [3,4]. To this end, the digital image processing procedure maps a rectangular grid onto the image. The grid points are characterized by their coordinates and by the gray scale distribution in their proximity. After straining, the pattern is recognized by image cross-correlation assuming that the gray scale distribution around a given coordinate remains constant during straining. From the change in border coordinates containing the correct initial gray scale distribution around the grid point, the 3-dimensional displacement gradient tensor field is determined at each grid point. These data serve as input for deriving the surface components of the local strain tensor. The strain tensor is used in the definition as the first order approximation of the standard polar decomposition of the displacement gradient tensor. The method may work with 2- or 3-dimensional surface coordinates. In the latter case, the coordinates are determined from

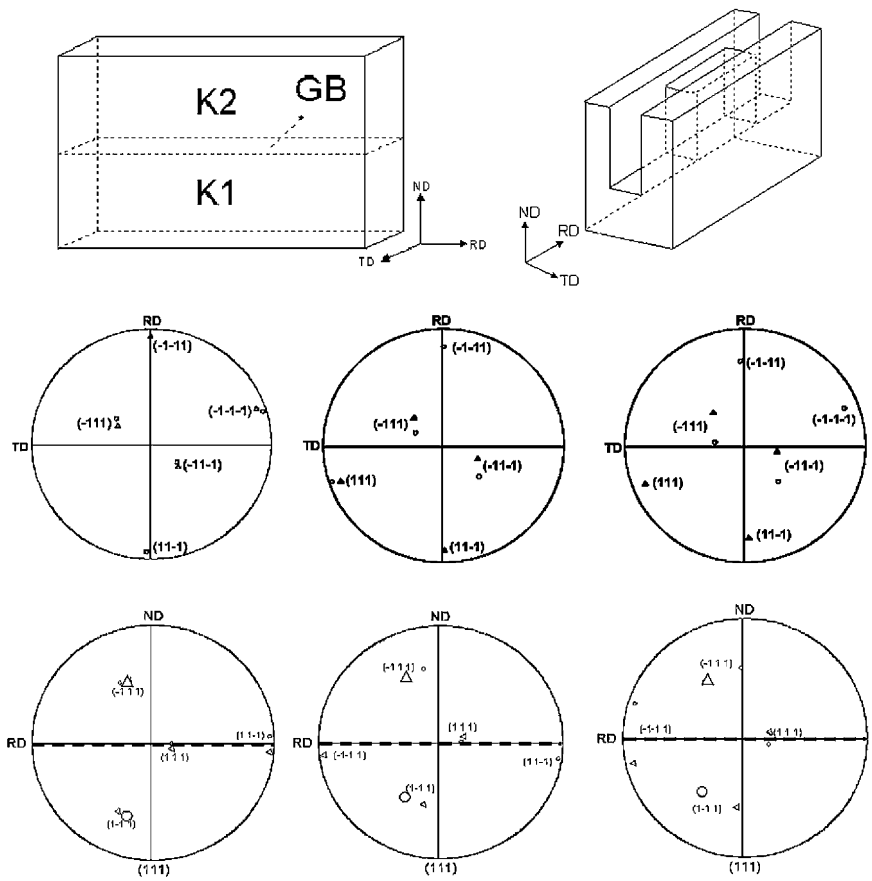

Fig. 1. (a) Schematic figure of the bicrystal and of the experimental set-up. (b) {1 1 1} pole figures of the initial bicrystals with symmetrical tilt grain boundaries of (a) 8.7° misorientation (b) 15.4° misorientation, and (c) 31.5° misorientation (○: crystal K1 and △: crystal K2) in TD/RD projections (upper row) and ND/RD projections (lower row). The large, filled symbols represent the principal slip systems.

stereo pair images of the sample. It should be pointed out that the photogrametric method works without any artificial regular grid on the sample surface. The spatial resolution of the method is, therefore, independent of any external grid size, but is of the order of the respective optical setup (12.5 μm in the present case), provided that the observed surface characteristics are sufficiently small. Both the natural characteristics of an unprepared sample surface or an artificial quasi-stochastic color spray applied to a polished surface may serve as input pattern. The strain resolution is below 1% since the method uses the match of the complete gray scale *distribution* before and after loading as a measure to determine the exact shift in border coordinates. This procedure provides a larger precision than the determination of the new border coordinates in the form of discrete pixel steps.

In the present study, a color spray was placed onto a polished sample surface. In order to avoid optical reflections the metallic surface was first primed with a white color spray. Second, fine dots of black color were placed on the white surface providing excellent contrast for pattern recognition. Images of the sample surface were acquired with a high resolution CCD camera and 2-dimensional displacement fields were determined.

2.3. Experimental determination of microtextures

The local lattice orientations were measured before and after plastic deformation by automatic crystal orientation mapping (ACOM) on the ND–RD plane of all bicrystals using automated acquisition and processing of electron back scatter diffraction patterns in a scanning electron microscope (SEM). High resolution maps of small areas across the grain boundary and in the bulk were determined in an SEM with field emission gun with high emission current (JSM 6500 F). The maps were measured with a step size of 50 nm on a surface area of $14 \times 35\ \mu m^2$.

3. Theoretical methods

3.1. Constitutive model for the crystal plasticity finite element simulations

In the large strain constitutive crystal plasticity model [32] used in the present work, one assumes the stress response at each macroscopic continuum material point to be potentially given by one crystalline volume point. The constitutive equation for the stress in each grain is then expressed in terms of

$$\mathbf{T}^* = \mathbf{C}\mathbf{E}^* \tag{1}$$

where $\mathbf{T}^*$ is the Cauchy stress produced by the crystalline portion, $\mathbf{C}$ is the fourth order elastic tensor, and $\mathbf{E}^*$ an elastic strain measure obtained by polar decomposition,

$$\mathbf{E}^* = \frac{1}{2}(\mathbf{F}^{*\mathbf{T}}\mathbf{F}^* - 1) \tag{2}$$

which leads to a stress measure, which is the elastic work conjugate to the strain measure $\mathbf{E}^*$,

$$\mathbf{T}^* = \mathbf{F}^{*-1}(\det(\mathbf{F}^*)\mathbf{T})(\mathbf{F}^*)^{-\mathbf{T}} \tag{3}$$

where $\mathbf{T}$ is the symmetrical Cauchy stress tensor in the grain, and $\mathbf{F}^*$ is a local elastic deformation gradient defined in terms of the local *total* deformation gradient $\mathbf{F}$ and the local *plastic* deformation gradient $\mathbf{F}^p$. The relation between the elastic and the plastic portion of $\mathbf{F}$ amounts to

$$\mathbf{F}^* = \mathbf{F}(\mathbf{F}^p)^{-1},\ \det(\mathbf{F}^*) > 0,\ \det(\mathbf{F}^p) = 1 \tag{4}$$

The plastic deformation gradient is given by the flow rule

$$\dot{\mathbf{F}}^p = \mathbf{L}^p\mathbf{F}^p \tag{5}$$

with $\mathbf{L}^p$ being the plastic flow rate. In crystals, $\mathbf{L}^p$ is composed of the superposition of the resolved crystallographic plastic shear rates, $\dot{\gamma}^\alpha$, such that

$$\mathbf{L}^p = \sum_\alpha \dot{\gamma}^\alpha \mathbf{S}_0^\alpha,\ \mathbf{S}_0^\alpha = \mathbf{m}_0^\alpha \otimes \mathbf{n}_0^\alpha \tag{6}$$

in which $\dot{\gamma}^\alpha$ is the shearing rate on the slip system α, and $\mathbf{m}_0^\alpha$ and $\mathbf{n}_0^\alpha$ denote the slip direction and the slip plane normal of the slip system, respectively, in the initial unloaded configuration. The shearing rate on each slip system depends on the resolved shear τ^α and the slip resistance s^α of that slip system and it is taken as

$$\dot{\gamma}^\alpha = \dot{\gamma}_0 \left| \frac{\tau^\alpha}{s^\alpha} \right|^{1/m} \operatorname{sign}(\tau^\alpha) \tag{7}$$

in which $\dot{\gamma}_0$ denotes a reference value of the slip rate and m represents the strain rate sensitivity parameter. In the present study, $\dot{\gamma}_0$ is taken as 0.001 s^{-1} and m is taken as 0.05. The evolution of the slip system resistance can be taken as

$$\dot{s} = \sum_\beta h^{\alpha\beta}|\dot{\gamma}^\beta|,\ h^{\alpha\beta} = q^{\alpha\beta}h^{(\beta)},\ h^{(\beta)} = h_0\left\{1 - \frac{s^\beta}{s_s}\right\}^a \tag{8}$$

where $q^{\alpha\beta}$ are the components of a matrix which describe the latent hardening behavior of the crystal, and h_0, a and s_s are slip system hardening parameters which are taken to be identical for all slip systems. For the twelve $\{1\,1\,1\}\langle 1\,1\,0\rangle$ slip systems of an FCC crystal (Table 1), we take $q^{\alpha\beta} = 1.0$, if the slip systems α and β are coplanar and $q^{\alpha\beta} = 1.4$ if they are not coplanar. An implicit crystal plasticity procedure proposed by Kalidindi et al. [32] was implemented and used for the time integration of the constitutive equations. Calculations were carried out using the finite element program ABAQUS in conjunction with the user defined material subroutine UMAT [33].

Table 1
Slip system notation

Plane	(111)			$(\bar{1}11)$			$(1\bar{1}1)$			$(11\bar{1})$		
Direction	$01\bar{1}$	$\bar{1}01$	$1\bar{1}0$	$01\bar{1}$	101	$\bar{1}\bar{1}0$	$01\bar{1}$	$\bar{1}01$	110	$01\bar{1}$	101	$\bar{1}10$
System	A1	A2	A3	B1	B2	B3	C1	C2	C3	D1	D2	D3

3.2. Application of homogenization models for the determination of the active slip systems

The active slip systems for the three bicrystals were additionally predicted by use of polycrystal and single crystal homogenization models [34–39] and compared to the results of the crystal plasticity finite element simulations. For this purpose, three single- and polycrystal models were selected, namely the no-strain-constraints Sachs approach (NC model) [39], the full constraints Taylor approach (FC model) [34,35], and a relaxed constraints Taylor approach (lath model) [36–38]. The Sachs or no-strain-constraints approach is a single crystal model, where simply those slip systems with the largest resolved shear stresses (orientation factor) are activated. The Taylor full constraint model prescribes the complete strain rate tensor imposed by the channel die experiment for each orientation, thereby accounting for strain rate compatibility among the neighboring crystal portions. The various Taylor relaxed constraint models prescribe only some of the external strain rate tensor components. This implies relaxation of the non-prescribed strain rate components among the neighboring crystal volumes partially dropping strain rate compatibility. In the present case, we used the lath relaxed constraints model, which relaxes the RD/ND shear component.

4. Results and discussion

4.1. Introduction

The results and their discussion will be separated in different subjects, namely, an estimation of the predominant slip systems, the macroscopic observation of shape change and strain distribution, the lattice rotations during the deformation experiment, the microtexture and microstructure, and finally, the influence of the grain boundary on the deformation behavior.

4.2. Characterization of the bicrystals before deformation

The investigated bicrystals have symmetric tilt boundaries with three different misorientations. Common tilt axis is in all cases the ⟨1 1 2⟩ crystal direction, which is parallel to TD. Fig. 1b shows the orientation of the crystals in (1 1 1) pole figures as viewed from TD. This observation direction has been adapted throughout the paper, because it shows best the symmetry of the two orientations. (1 1 1) pole figures are chosen, because the (1 1 1) planes correspond to the glide planes in the material. In the pole figures, those planes are highlighted, which belong to the glide system with the highest Schmid factor, i.e. with the largest or resolved shear stress for the given stress tensor which was chosen to be equal to the macroscopic deformation tensor. The Schmid factors for all glide systems are shown in Table 2 together with values for the amount of shear on these glide systems obtained by Taylor and CPFEM calculations for all three samples.

4.3. Macroscopic observations (shape change and strain distribution)

Fig. 2 shows the accumulated plastic von Mises strain distribution of the three bicrystals after 30% thickness reduction in the channel die experiment as measured via photogrametry. Each experimental figure is contrasted with the corresponding crystal plasticity simulation result. In order to indicate the position of the glide planes the (1 1 1) pole figures after deformation are also added to each bicrystal image. Although some differences between experi-

Table 2
Theoretical predictions for crystallographic shear in the bicrystals with (a) 8.7°, (b) 15.4° and (c) 31.5° symmetrical ⟨1 1 2⟩ tilt grain boundary. Comparison of the shear contributions (in percent of the total shear on all systems) as predicted by the different plasticity models. FEM: crystal plasticity finite element simulation, FC: full constraints Taylor model, lath: relaxed constraints Taylor model with relaxation of the RD/ND shear component, Sachs: single crystal model using the system(s) with the largest orientation (Schmid) factor

Slip system	K1				K2			
	FEM	FC	Lath	Sachs	FEM	FC	Lath	Sachs
(a) 8.7°								
A1	21.5	26.5	18.0	0.110	12.35	25.8	19.2	0.084
A2	9.48	12.3	13.3	0.050	20.28	12.7	11.3	0.071
A3	0	0	0	0.060	0	0	0	0.008
B1	2.98	20.9	0	0.331	**54.8**	**34.3**	**60.6**	**0.398**
B2	0.05	0	0	0.303	1.09	0	0	0.278
B3	0.04	0	0	0.027	0.21	0	0	0.119
C1	0.27	7.9	0	0.243	0.13	7.9	0	0.270
C2	**62.11**	**32.4**	**62.5**	**0.398**	10.41	19.3	0	0.333
C3	2.19	0	0	0.155	0	0	0	0.062
D1	1.23	0	6.2	0.022	0.13	0	0	0.043
D2	0.04	0	0	0.045	0.41	0	8.9	0.021
D3	0.1	0	0	0.067	0.17	0	0	0.064
(b) 15.4°								
A1	20.55	22.1	11.4	0.095	15.9	12.2	11.9	0.054
A2	10	18.5	18.3	0.083	17.43	28.1	18.7	0.121
A3	0.01	0	0	0.011	0	0	0	0.067
B1	4.29	7.6	0	0.264	**55.88**	**33.9**	**60.6**	**0.405**
B2	0.12	0	0	0.264	2.05	10.2	0	0.234
B3	0.23	0	0	0	0.11	0	0	0.171
C1	1.08	10.5	0	0.253	0.22	0	0	0.301
C2	**55.49**	**41.3**	**58.6**	**0.418**	5.41	15.6	0	0.304
C3	1.81	0	0	0.164	0	0	0	0.003
D1	3.02	0	11.7	0.084	0.21	0	0	0.049
D2	0.37	0	0	0.069	2.74	0	8.8	0.051
D3	3.03	0	0	0.153	0.05	0	0	0.101
(c) 31.5°								
A1	15.39	19.3	15.5	0.13	4.05	13.1	12.3	0.049
A2	1.58	12.9	12.6	0.03	18.16	26.7	16.1	0.128
A3	1.86	0	0	0.099	0.25	0	0	0.079
B1	1.02	0	0	0.15	**43.76**	**46.2**	**57.6**	**0.428**
B2	0.59	0	0	0.281	0.58	11.4	0	0.206
B3	5.35	0	0	0.131	9.2	0	0	0.222
C1	0.52	4.1	0	0.181	0.19	0	0	0.285
C2	**33.05**	**53.2**	**57.3**	**0.433**	4.83	0	0	0.202
C3	6.75	0	0	0.252	1.99	0	0	0.082
D1	6.13	10.4	14.7	0.161	1.41	0	0	0.093
D2	0.32	0	0	0.121	5.9	2.4	14.1	0.132
D3	27.44	0	0	0.283	9.69	0	0	0.225

ment and simulations are visible, it is striking how well most features of the experiment are matched by the simulation. This similarity gives some confidence in the calculated amounts of shear for the different glide systems (Table 2(a) for the 8.7° bicrystal, Table 2(b) for the 15.4° bicrystal, and Table 2(c) for the 31.5° bicrystal) and can be used for interpretations in the following chapters. All bicrystals show a characteristic shape change where both abutting crystals shear in the same

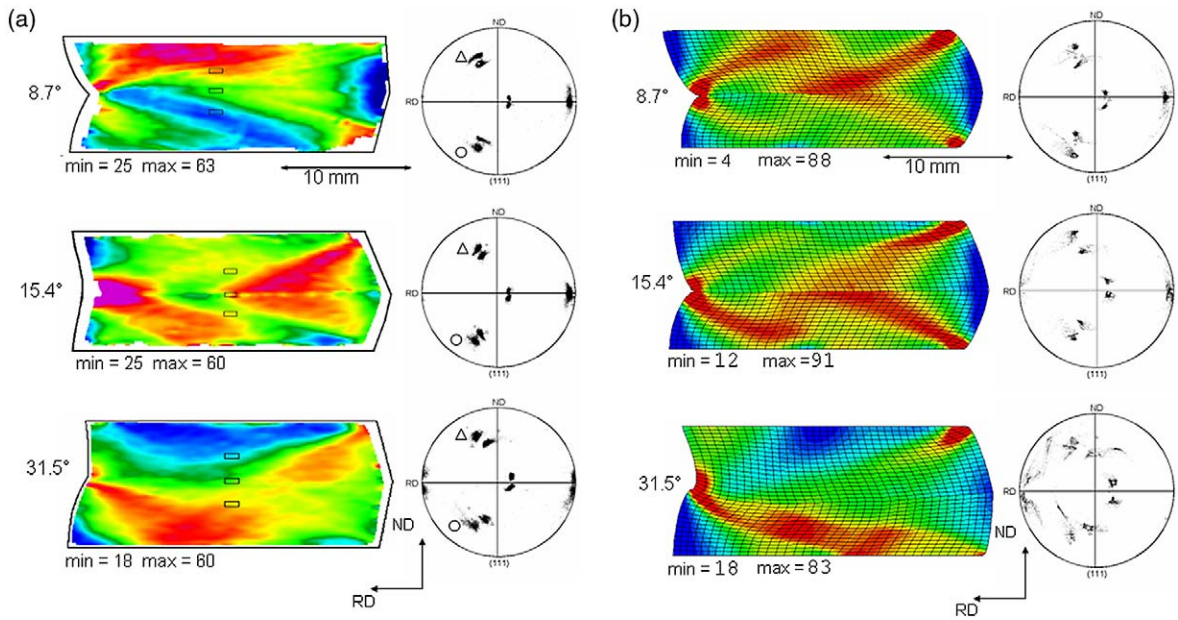

Fig. 2. The spatial distributions of the von Mises strain obtained (a) by measurement and (b) simulation for the 30% deformed aluminum bicrystals. Red color marks areas of maximum strain, blue color those of minimum strain. The minimum and maximum values are given in the form of an engineering strain measure.

direction, showing approximate mirror symmetry to each other as the orientations. Also, all bicrystals show strong deformation heterogeneities in the form of macroscopic shear localizations. These localizations are not completely mirror symmetric with respect to the grain boundary. This observation can be attributed to the slightly different size of the abutting crystals, leading to different deformation geometry on either side of the grain boundaries.

Principally, the observed external shape change and the internal deformation heterogeneities are due to the interplay of continuum effects and crystalline effects. The principle of shape formation of the bicrystal is sketched in Fig. 3. The bicrystal is separated into two single crystals of symmetric orientation. For simplicity, it is assumed that only one glide system is active. Its glide planes are indicated by thin lines. The thick arrows indicate the desired material movement during plane strain compression. In the two opposite corners on the one side, material movement and glide plane position coincide so that strong glide will occur. In the other two corners, glide plane and material movement are in different directions and glide is inhibited. The result of this situation is that the corners with strong glide activation move ahead, while the corners with little glide stay behind entailing the shape change observed. Since both crystals glide on symmetric glide planes their shape also develops in a symmetrical sense. The sketch shows that, the observed shape of the bicrystal is not principally due to bicrystal deformation, but can also be (approximately) explained by the deformation of two separated single crystals [24–29]. The shape change should become less evident when more than one glide system is activated. This can be actually observed in the present case: the different simulations show that in the case of the 8.7° (Table 2(a)) and 15.4° (Table 2b) bicrystals one glide system has a much larger shear fraction than the other system, while in the 31.5° bicrystal (Table 2(c)), the predominance of one slip system is less pronounced. This corresponds to the observation that the double-rhombus shape of the 31.5° bicrystal is less pronounced when compared to the shapes of the 8.7° and 15.4° specimens (Fig. 2).

The next aspect which deserves a closed analysis

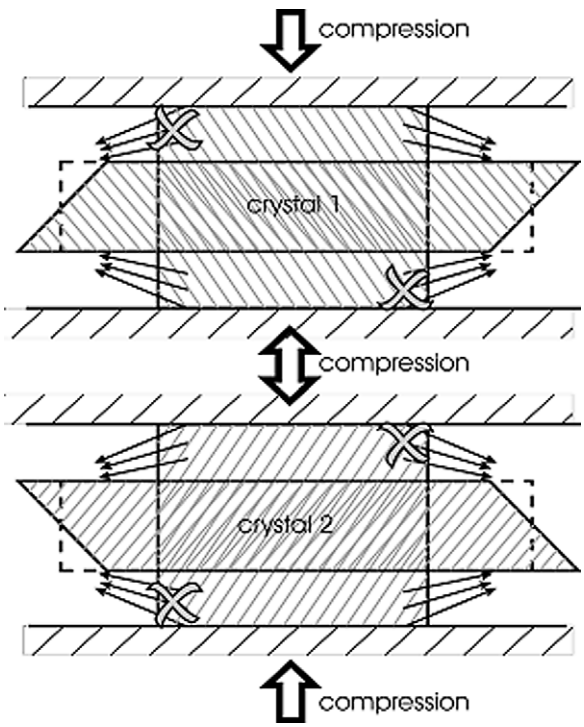

Fig. 3. Schematic drawing of the crystalline and macroscopic kinematics, explaining the shape formation of the bicrystals.

are the observed macroscopic shear bands. From isotropic J2-based continuum mechanics it is well known that the friction between tool and sample in a compression experiment leads to the formation of shear localizations entering the material at each corner under a certain degree with respect to the compression axis [40]. The same effect also appears in our samples, but it overlaps with the crystalline effects outlined above. Fig. 4 sketches the effect for the same simplified model as described above, i.e. only one glide system is assumed to be active. One of the crossing macroscopic shear bands coincides with the glide plane position and, therefore, leads to strong local deformation. The other one lies under a large angle to the glide planes and, hence, does not occur. Due to the symmetric orientation of the second crystal, its glide situation is inversed and the macroscopic shear bands do not penetrate into the opposite crystal. The large aspect ratio of our present compression test (compressed length/thickness) prohibits that the macroscopic shear bands continue to

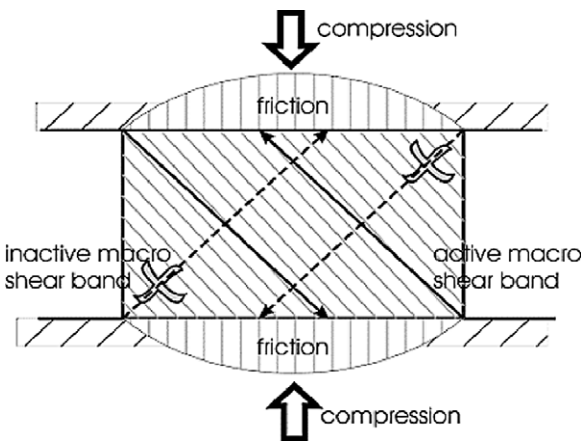

Fig. 4. Schematic drawing of the overlap of crystalline and macroscopic effects, explaining the formation of macroscopic shear bands in a single crystal.

the respectively opposite corner. Rather, they are stopped half way when reaching the interface. This effect promotes the formation of two almost parallel shear bands starting from the two opposite corners. Depending on the orientation of the active glide system, the macroscopic bands are more or less strongly deflected from their isotropic J2-based continuum mechanical position. In the 31.5° bicrystal the primary glide planes are most strongly inclined to the compression surface and the macroscopic shear bands, therefore, run under the smallest angle through the crystal (Fig. 2).

It can be concluded from the observation of shape and shear localizations that the bicrystals behave to a large extent like two individual single crystals [24–29]. The grain boundary largely acts like a surface in direct contact with the compression tool and strong friction on it. Our results substantiate that the observed macroscopic shape change behavior of the samples is essentially governed by the crystallographic kinematics of the crystals. Although, the low angle bicrystal interface is principally penetrable for mobile dislocations the kinematics of the two abutting crystals do not promote the translation of slip from one grain to the other owing to their individual slip behavior.

The observed strong heterogeneities of the macroscopic strain distribution (and therefore also of the crystal rotations) and the slight deviations

between experiment and model which can be attributed to unknown details such as the exact friction coefficient and the exact size relation between the abutting crystals make it questionable whether it is possible to determine the small effects that might be caused by a change in the grain boundary structure.

4.4. Lattice rotations

Lattice rotations have been measured by ACOM on different lateral scales ranging from the complete ND–RD surface of the bicrystal in the order of several 10 mm^2 to regions close to grain boundary in the range of few μm^2. The goal of these measurements was to separate the bulk behavior of the two crystals from the behavior close to the grain boundaries. Owing to the strong strain heterogeneities, the lattice rotations are also heterogeneously distributed over the sample surface. This effect makes it difficult to choose *representative* and similar mechanical areas in the different bicrystals. Therefore, in order to get a first impression about the macroscopic *average* lattice rotation, Taylor calculations were carried out for all three bicrystals. Taylor simulations do not include any constitutive element for describing deformation heterogeneity. In order to check the reliability of these simulations they were, therefore, compared with the CPFEM simulations with respect to the type and amount of activated glide systems (Table 2(a–c)). The data underlines that the basic tendency is very similar in different approaches. Surprisingly, the results of the full constraint calculations fit better to the CPFEM results, than those obtained by the lath model.

The pole figures showing the rotation paths as calculated with the FC Taylor model are displayed in Fig. 5 revealing some general tendencies. For all bicrystals, the sense of rotation and its magnitude is about the same for the two abutting crystals. The rotation axes is in all cases close to the transverse direction, but does not coincide with it. Due to the different start orientations, the misorientations develop differently. For the 8.7° bicrystal, the crystals rotate away from each other, so that the misorientation increases. The 15.4° and 31.5° bicrystals first rotate towards and then away from each other, thereby slightly increasing the final misorientation in the case of the 15.4° bicrystal and keeping it about constant in the case of the 31.5° bicrystal. A comparison of the FC Taylor simulations with the CPFEM simulations shows two significant differences. First, in the CPFEM calculations the crystal rotations are smaller. Second, they lead to a spatial orientation distribution for each crystal (details of the local textures will be discussed in the next chapter).

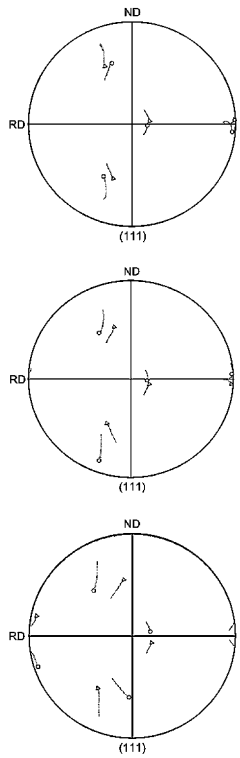

Fig. 5. Pole figures showing the rotation paths as calculated by FC Taylor theory. The triangle and circle symbols mark the initial crystal orientation.

Finally, in the experimental data the average rotations[2] are still smaller and the final orientation spread is narrower than in the CPFEM calculations. Similar observations have been made, for

[2] Average orientations have been determined from experimental data and from CPFEM calculations as the maximum of the ODF of the respective single crystals. In both cases, the extreme ends of the bicrystals and particularly the corners with strong shear localizations have been excluded from the analysis.

example, by Becker and Panchadeswaran [41]. Due to the smaller rotation rates, the final experimental misorientations differ from those obtained in the simulations. The experiments show that the misorientation increases for the 8.7° bicrystal, it remains almost constant for the 15.4° bicrystal, and it decreases for the 31.5° bicrystal during straining.

It is very likely though, that the differences in crystal reorientations observed for the different bicrystals are due to the different starting orientations and not to the influence of different grain boundary misorientations. The data suggest that the grain boundaries themselves are independent of their misorientation, rather stiff and kinematically inactive. The influence of a grain boundary on the crystal rotation should, therefore, be relatively small and, as a consequence, difficult to measure. Unfortunately, the experimental determination of crystal rotations is subject to relatively large experimental errors, particularly due to possible sample rotations by dismounting and remounting the sample from the microscope stage for the deformation experiment. Absolute sample rotations with respect to the undeformed crystal could therefore not be measured with sufficient precision. Instead, we determined *relative* rotations, i.e. misorientations with respect to the average crystal orientation. They will be discussed in the ensuing section.

4.5. Microtexture and microstructure

In contrast to the crystal rotation rates which characterize the change in orientation *during* straining, microtexture mappings characterize the spatial and angular distribution of orientations *after* the deformation process. The crystal does not rotate as a whole but splits up into different orientations at different positions on the sample. This separation occurs on two different length scales. The heterogeneous strain distribution leads to orientation variations at the millimeter scale (see pole figures in Fig. 2). These orientation variations are also predicted by the CPFEM simulation. The simulated pole figures (Fig. 2b) show much larger orientation variations than observed in experiment [41].

To some extent, this deviation from experiment can be caused by the fact that the simulations were carried out without re-meshing, although this would have been necessary particularly at the corners, where heavy strain localization entailed strong mesh deformation. A second cause can be seen in the generally larger reorientation rates in simulations when compared to experiments [41].

From the measurements displayed in Fig. 2a, areas with similar accumulated von Mises strains in all three bicrystals were selected for microstructure and texture determination by ACOM. The position of these areas are shown in the figures in the form of small rectangles. The orientation maps obtained from these areas and the corresponding (1 1 1) pole figures are presented in Fig. 6. All orientation maps reveal the existence of a second kind of orientation heterogeneities on the length scale of micrometers. Particularly, the 8.7° bicrystal (but less significant also the other two samples) reveal the formation of regular orientational block patterns. The blocks consist of regions of alternating lattice rotations with respect to the average orientation of the whole area. The axis of this orientation spread is close to the transverse direction and the spread amounts to about 10°. These observations correspond well to earlier studies on the microtextures of aluminum single crystals [24–29]. The formation of these orientational block patterns can be explained in terms of the activation of alternating sets of glide systems in different regions of the crystal. The different active glide systems in the different regions lead to different crystal rotations and, therefore, to formation of blocks as described, for example, in [24–29]. According to the classical homogenization picture of Taylor [34], Bishop and Hill [35], at least five glide systems have to be activated everywhere in the crystal, in order to accommodate the prescribed macroscopic strain for obvious grain scale compatibility reasons. Five glide systems, however, have been very rarely found to act simultaneously in real crystals. In fact, it can be assumed that the activation of more than three glide systems quickly leads to strong entanglement of dislocations and is, therefore, rather improbable. Instead, small neighboring regions deforming alternating by different combinations of small sets of active glide systems, can also accommodate all required degrees of free-

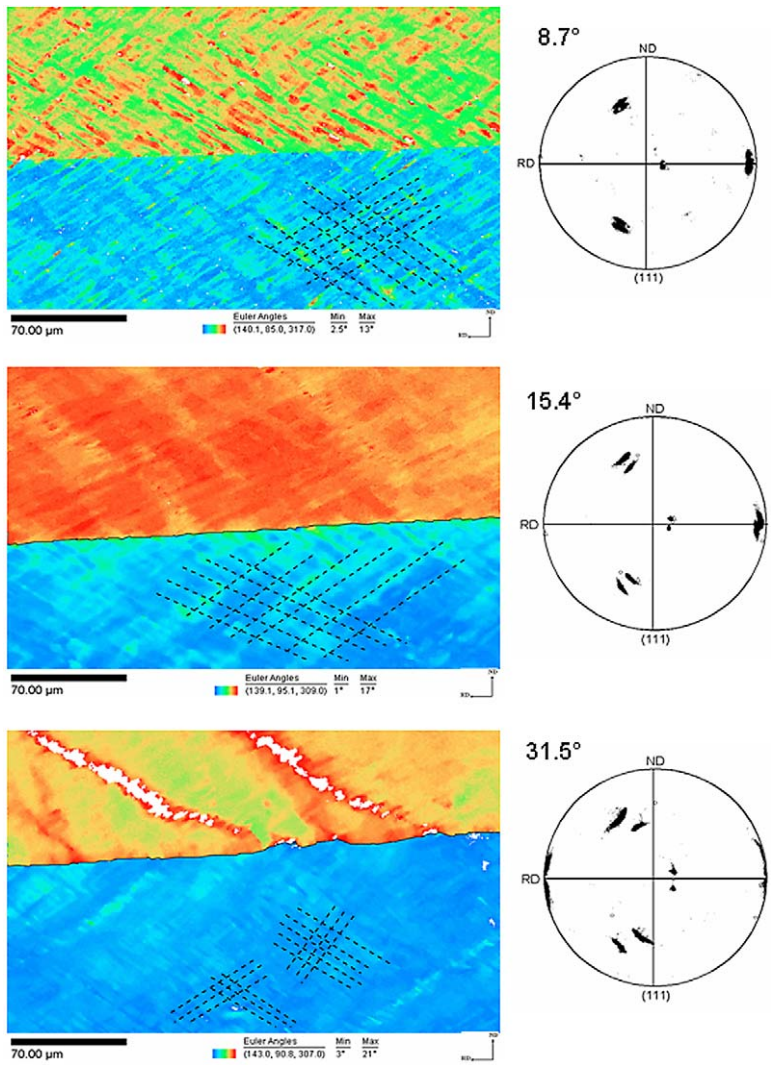

Fig. 6. High resolution orientation maps close to the grain boundaries in zones of similar von Mises strain (see rectangles in Fig. 2a) and corresponding (1 1 1) pole figures. Dotted lines line out the spatial orientation and size of orientational block patterns.

dom over a volume which exceeds the zones occupied by just one of those sets. This means such alternating plastic regions can, as a whole, fulfill the requirements of classical homogenization theory. As was reported earlier by other authors [24–29], the size of these regions of different glide system combinations depends on the strain and stress level and as well as on the orientation of the crystal.

Visual rating of the block sizes formed in the three bicrystals (visualized in Fig. 6 by lines parallel to some of the block boundaries) reveals the following details. The 8.7° bicrystal shows the sharpest blocks. The blocks in the 15.4° bicrystal are less sharp and their size exceeds that of those observed in the 8.7° bicrystal. Finally, the 31.5° bicrystal shows very small block sizes and, additionally, the formation of shear bands. These observations fit well into the picture given of orientational block pattern formation outlined above. The data are also in line with the shear rate simulation data given in Table 2(a–c). The simulations

for the 8.7° (Table 2(a)) and the 15.4° bicrystals (Table 2(b)) show a strong dominance of single slip. This effect leads to long and rather homogeneous elongated orientation bands (Fig. 6). Although basically similar, the bands in the 8.7° bicrystal are narrower than those in the 15.4° sample. This variation can be attributed to possible variations in the local micromechanics (Fig. 2a). In contrast, the 30° bicrystal shows a significantly larger amount of poly slip which leads to very small block sizes. It may be assumed that due to the high amount of poly slip strong dislocation entanglement will occur leading to increased hardening of normal slip systems and to shear band formation as a further deformation mode.

It can be concluded that the observed microstructures and microtextures are due to the amount of polyslip activated in the crystals and, therefore, due to the orientation of the crystals. A certain tendency can be observed which states that an increasing amount of polyslip entails smaller blocks, each formed by regions of activation of different combinations of glide systems.

At first sight, the microstructure does not show any evidence for the influence of the grain boundary on the kinematics of deformation as was also stated for rotations and strain distribution. It should be mentioned, finally, that the crystal plasticity finite element simulations are not capable of reproducing block pattern structures, because of the relatively coarse mesh size and the linearity of the element interpolation function. Furthermore, it is very likely that the prediction of rapidly alternating orientation block patterns in a FE method might require the incorporation of adequate and physically sensible strain gradient terms into the constitutive description, reflecting geometrically necessary dislocations.

4.6. *Effect of grain boundaries*

The above discussion has shown that most of the observed differences between the three deformed bicrystals are due to the different orientations of these crystals and not due to the changing structure of the grain boundaries. The question is, whether there is any detectable effect that might relate directly to the grain boundary structure. It is clear that this effect must be small and that it is, therefore, difficult to observe under such heterogeneous boundary conditions. However, as will be shown in the following, some effects of the grain boundaries on the lattice rotation can be observed in areas of macroscopic homogeneity provided microscopic heterogeneity can be leveled out by using a suitable averaging method.

Already a careful visual inspection of the orientation maps given in Fig. 6 reveals a change in color, i.e. in orientation close to the grain boundaries. In order to quantify these orientation changes, the misorientation of each measurement point with respect to a fixed reference orientation was calculated. As reference, the average orientation of the whole area was chosen. Subsequently, the average misorientation of all points along straight lines parallel to the grain boundary was determined by calculating the arithmetic mean of the misorientation angle of these points. This simple way of averaging is permitted only because the misorientation angles are small (of the order of 5°) and the misorientation axes are close to each other. The results of these calculations are presented in Fig. 7 in the form of an average misorientation angle, as a function of the distance from the grain boundary. The scatter bars show the standard deviation for each averaged data set. The analysis shows that for all three bicrystals, a change of orientation occurs on either side of the grain boundary. The changing lattice rotation extends into the crystal over a distance of about 10 μm. The 8.7° bicrystal shows virtually no effect when getting close to the grain boundary. The 15.4° bicrystal, in contrast, shows quite a strong orientation gradient effect. Close to the grain boundary, the misorientation to the average orientation is on both sides of the boundary about twice as high as in the bulk material far away from the interface. A deviating orientation is measured up to a distance to the grain boundary of almost 20 μm on either side of the boundary. For the 31.5° bicrystal, the analysis is more difficult, because shear bands cross the orientation maps and create a large data scatter. Also, the grain boundary does not remain flat in those areas where a shear band meets the grain boundary. These regions were hence omitted from the averaged areas. The curves show that in

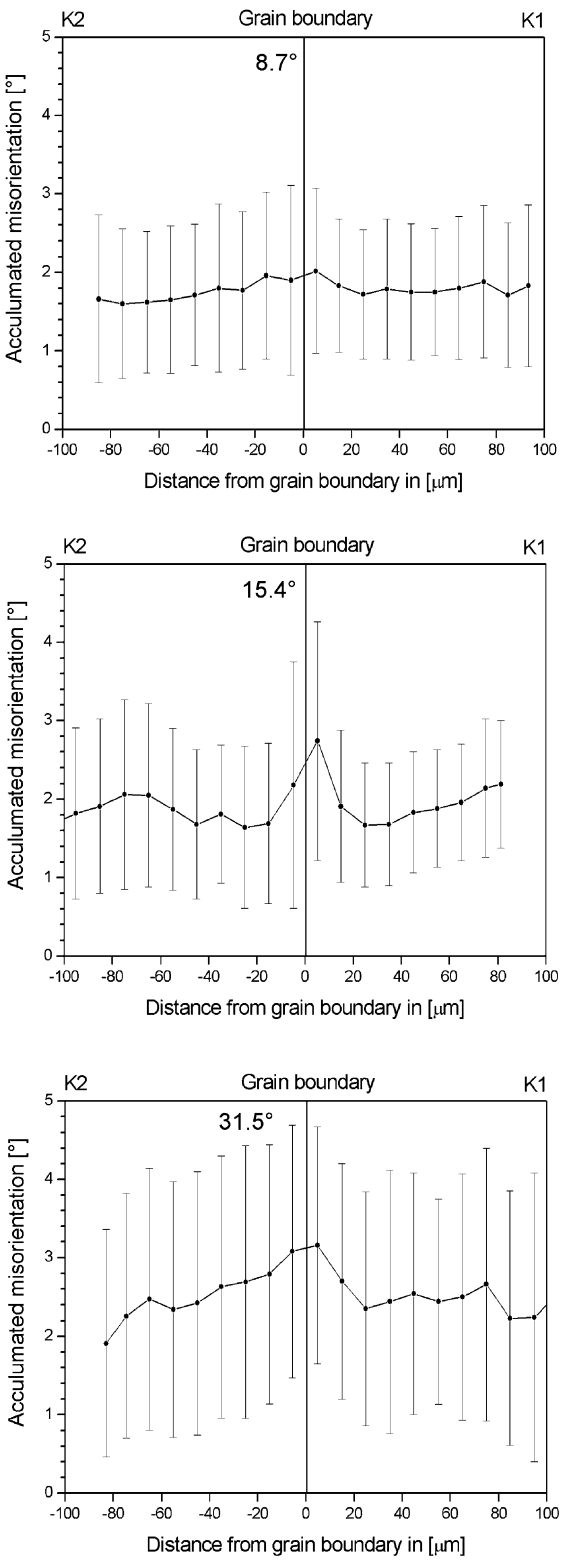

this case, the effect of the grain boundary is smaller than for the 15.4° boundary. The average misorientation close to the grain boundary is only increased by a third of the bulk misorientation. Instead, it seems that the mechanical effect extends deeper into the bulk material up to a distance of almost 30 μm on either side.

The observed crystal rotations may be due to two different, superimposed effects. One effect is a homogeneous rotation in the sense of Taylor [34]. Rotations of this type are due to dislocations that have completely passed through the crystal and are responsible for the average lattice reorientation of the crystals. The axis of this lattice rotation is perpendicular to the glide plane normal and the glide direction. The sense of rotation is such that the glide plane normal moves towards the compression direction (see also the sketch about the bicrystal deformation in Fig. 3). The second effect is the rotation due to dislocation pile-ups. These dislocations bend the crystal lattice in exactly the opposite sense as that one created by the Taylor rotation. In contrast to the Taylor-type rotations, the pile-up rotations build up large elastic stresses and have, therefore, only a limited spatial extension. If the stresses become too large, dislocation sources in the boundary or in the neighboring crystal are activated and dislocations are emitted into the abutting crystal. In the bicrystal geometry adapted here, these dislocations themselves should reduce the lattice rotations that have been built-up on that side of the grain boundary into which they are emitted.

The observation that pile-ups and the resulting reorientation gradients are small for the low angle grain boundary and large for the grain boundaries with higher misorientation between the crystals fits well into standard conceptions of grain boundary mechanics. The smaller the misorientation angle is, the easier it is for a dislocation to penetrate through the boundary and the less pile-ups are formed. The fact that the 31.5° grain boundary shows a smaller rotation, but a deeper pile-up of orientations might

Fig. 7. Misorientation with respect to the average crystal orientation integrated over narrow stripe-shaped areas parallel to the grain boundary in dependence of the distance of the integration area to the grain boundary.

be explained by the much higher degree of polyslip in the abutting crystals compared to the 15.4° bicrystal. In a polyslip situation, the different activated glide systems may lead to different reorientations involving a certain probability that antisymmetric slip portions mutually compensate. The net rotation directly in front of large angle grain boundaries may in some cases, therefore, be relatively small. Due to the strong dislocation interaction in case of polyslip it is also likely that dislocations are impeded and entangled earlier in front of the grain boundary so that dislocation gradient accumulation may reach deeper into the bulk crystal.

It can be concluded from the observations presented in this study that it cannot be decided with certainty whether the observed effects are due to a change in grain boundary structure or due to the changing orientation of the abutting crystals. A good way to tackle this problem would be a detailed comparison of a larger number of spatially averaged experimental results with precise simulations, provided that the simulations give exactly the correct average lattice reorientations. This is, however, not yet fully the case for the current models.

5. Conclusions

Aluminum bicrystals with different misorientations have been deformed in a channel die experiment in order to study the influence of misorientation on the kinematics of deformation zones around grain boundaries. The deformation behavior of the samples has been characterized on a macroscopic level by strain distribution measurements and on a microscopic level by automatic crystal orientation mapping in the scanning electron microscope. The experiments were supported by simulations with a crystal plasticity finite element model in order to calculate the shear fractions on the different activated glide systems. The macroscopic strain data revealed that channel die deformation of bicrystals leads to pronounced strain heterogeneity created by an overlap of J2-type frictional continuum and crystal plasticity effects. The observed degree of heterogeneity suggests that channel die deformation is not an optimal approximation of a plain strain deformation state. The use of a novel strain measurement technique allowed us to identify areas of locally homogeneous strain. These were investigated in detail by automatic crystal orientation mapping. These measurements showed the existence of further microstructural heterogeneities at the micrometer scale. These heterogeneities, consisting of blocks of different orientations with misorientations in the range of 10°, are supposed to be due to the activation of different combinations of glide systems in neighboring regions. We found that most of the observed features of these orientational block patterns, i.e. block size, block misorientation and spatial orientation can be explained by the orientation of the individual crystals. In particular, it is assumed that the amount of single respective polyslip is responsible for the observed differences between the crystals. Besides the different kinematic mechanisms which we attributed either to macroscopic or crystallographic effects, the direct influence of the grain boundaries could be detected in the form of slight orientation changes in their vicinity. To render these changes visible, the orientation distances of each orientation point of a crystal with respect to the average crystal orientation were calculated and integrated over small stripe-shaped areas parallel to the grain boundary. The small angle grain boundary with 8.7° misorientation did not show any detectable effect. This was interpreted in terms of free penetration of dislocations through the boundary without any pile-up formation. In contrast, the 15.4° bicrystal showed a strong change of orientation close to the boundary. The orientation change started at a distance of about 20 μm on either side of the boundary and accumulated about 2° of misorientation. The 31.5° bicrystal also showed an orientation effect, but the orientation change started already in a distance of almost 30 μm and accumulated only about 1° of misorientation. The orientation change was interpreted as a dislocation pile-up in front of the impenetrable boundary.

References

[1] Rey C. Rev Phy Appl 1988;23:491.
[2] Delaire F, Raphanel JL, Rey C. Acta Mater 2000;48:1075.

[3] Raabe D, Sachtleber M, Zhao Z, Roters F, Zaefferer S. Acta Mater 2001;49:3433.
[4] Sachtleber M, Zhao Z, Raabe D. Mater Sci Eng A 2002;336:81.
[5] Chalmers B. Proc R Soc 1937;A162:120.
[6] Kawada T. J Phy Soc Jpn 1951;6:362.
[7] Gilman JJ. Acta Metall 1953;1:426.
[8] Aust KT, Chen NK. Acta Metall 1954;2:632.
[9] Clark R, Chalmers B. Acta Metall 1954;2:80.
[10] Livingston JD, Chalmers B. Acta Metall 1957;5:322.
[11] Fleischer RL, Chalmers B. Trans AIME 1958;212:265.
[12] Miura S, Saeki Y. Acta Metall 1978;26:93.
[13] Rey C, Zaoui A. Acta Metall 1980;28:687.
[14] Sun S, Adams BL, King W. Phil Mag A 2000;80:9.
[15] Yu P, Havner KS. J Mech Phy Sol 2001;49:173.
[16] Hauser JJ, Chalmers B. Acta Metall 1961;9:802.
[17] Mote JD, Dorn JE. Trans AIME 1960;218:491.
[18] Hook RE, Hirth JP. Acta Metall 1967;15:535.
[19] Hook RE, Hirth JP. Acta Metall 1967;15:1099.
[20] Chuang YD, Margolin H. Metall Trans 1973;4:1905.
[21] Lee TD, Margolin H. Metall Trans 1977;8A:145.
[22] Rey C, Zaoui A. Acta Metall 1982;30:523.
[23] Kröner E. Kontinuumstheorie der Versetzungen und Eigenspannungen. Berlin: Springer Verlag, 1959.
[24] Wert JA, Liu Q, Hansen N. Acta Mater 1997;45:2565.
[25] Godfrey A, Juul Jensen D, Hansen N. Acta Mater 1998;46:823.
[26] Hansen N, Huang X. Acta Mater 1998;46:1827.
[27] Godfrey A, Juul Jensen D, Hansen N. Acta Mater 2001;49:2429.
[28] Maurice C, Driver JH. Acta Mater 1997;45:4627.
[29] Basson F, Driver JH. Acta Mater 2000;48:2101.
[30] Winning M, Gottstein G, Shvindlerman LS. Mater Sci Eng A 2001;317:17.
[31] Winning M, Gottstein G, Shvindlerman LS. Acta Mater 2001;49:211.
[32] Kalidindi SR, Bronkhorst CA, Anand L. J Mech Phys Solids 1992;40:537.
[33] ABAQUS/Standard User's Manual, Volume II, 14.1.4-1, Hibbitt, Karlsson and Sorensen, Pawtucket (RI), 1999.
[34] Taylor GI. J Inst Met 1938;62:307.
[35] Bishop JFW, Hill R. Phil Mag 1951;42:414.
[36] Honneff H, Mecking H. In: Gottstein G, Lücke K, editors. Proceedings of the Fifth International Conference on Textures of Materials (ICOTOM 5). Springer Verlag; 1978. p. 265.
[37] Van Houtte P. In: Nagashima S, editor. Proceedings of the Sixth International Conference on Textures of Materials (ICOTOM 6). Iron and Steel Institute of Japan; 1981. p. 428.
[38] Raphanel JL, Van Houtte P. Acta Metall 1985;33:1481.
[39] Sachs G. Z Ver Dtsch Ing Ingen 1928;72:734.
[40] Backofen WA. Deformation processing. Addison-Wesley Publishing Company, 1972 Reading.
[41] Becker R, Panchanadeeswaran S. Acta Metall Mater 1995;43:2701.